THE PATH TO 1 MW: BEAM LOSS CONTROL IN THE J-PARC 3-GeV RCS

H. Hotchi#, H. Harada, S. Kato, M. Kinsho, K. Okabe, P.K. Saha, Y. Shobuda, F. Tamura, N. Tani, Y. Watanabe, K. Yamamoto, M. Yamamoto, and M. Yoshimoto
J-PARC Center, Japan Atomic Energy Agency, Tokai, Naka, Ibaraki, 319-1195 Japan

Abstract

The J-PARC 3-GeV RCS started a 1-MW beam test in October 2014, and successfully achieved a 1-MW beam acceleration in January 2015. Since then, a large fraction of our effort has been concentrated on reducing and managing beam losses. In this paper, recent progresses of 1-MW beam tuning are presented with particular emphasis on our approaches to beam loss issues.

INTRODUCTION

The J-PARC 3-GeV rapid cycling synchrotron (RCS) is the world's highest class of high-power pulsed proton driver aiming for a 1-MW output beam power. As shown in Fig. 1, a 400-MeV H^- beam from the injector linac is delivered to the RCS injection point, where it is multi-turn charge-exchange injected through a 340-μg/cm^2-thick carbon foil over a period of 0.5 ms. RCS accelerates the injected protons up to 3 GeV with a repetition rate of 25 Hz. Most of the 25-Hz pulses are transported to the material and life science experimental facility (MLF), while only 4 pulses every several seconds are delivered to the following 50-GeV main ring synchrotron (MR).

Recently injector linac upgrades were completed, by which the injection energy was upgraded from 181 MeV to the design value of 400 MeV in 2013, and then the injection peak current was increased from 30 mA to the design value of 50 mA in 2014. Via these series of the injector linac upgrades, RCS now has all the hardware parameters to realize its design performance.

Figure 2 shows the history of the RCS beam operation. RCS was beam commissioned in October 2007 [1] and made available for the user program in December 2008 with an output beam power of 4 kW. Since then, the RCS beam power ramp-up has steadily proceeded following progressions in beam tuning and hardware improvements [2, 3]. The output beam power for the routine user program has been increased to 500 kW to date, though it is temporarily limited to 200 kW at present due to a malfunction of the neutron production target at MLF. In addition to such a routine user operation, RCS has intermittently been continuing high-intensity beam tests toward realizing the design output beam power of 1 MW. As shown by red bars in Fig. 2, RCS started a 1-MW beam test in October 2014 right after completing the injector linac upgrades, and successfully achieved a 1-MW beam acceleration in January 2015.

The most important issue in realizing such a MW-class high-power routine beam operation is to keep machine activations within a permissible level, that is, to preserve a better hands-on-maintenance environment. Thus, a large fraction of our effort has been concentrated on reducing and managing beam losses. This paper presents recent progresses of 1-MW beam tuning especially focusing on our approaches to beam loss issues.

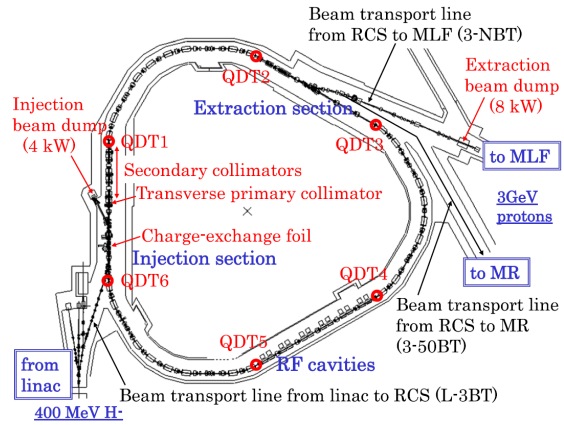

Figure 1: Layout of the J-PARC 3-GeV RCS.

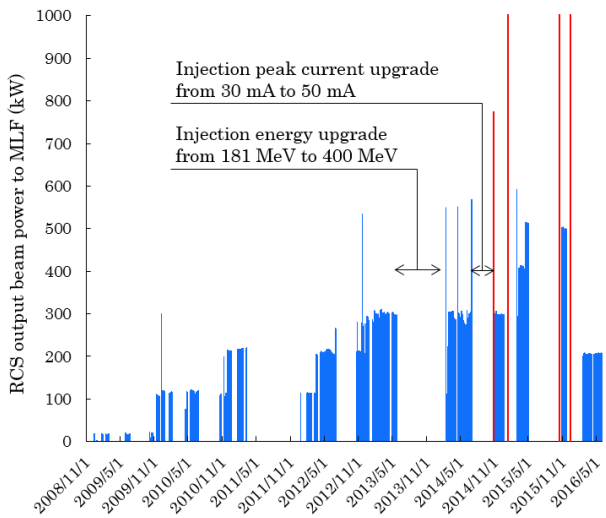

Figure 2: History of the RCS beam power since the start-up of the user program in December 2008.

RESULTS OF THE INITIAL STAGE OF THE 1-MW BEAM TEST

Longitudinal Beam Loss and its Mitigation

As already reported in the last HB workshop [3], the first 1-MW beam test was conducted in October 2014. In this trial, the beam acceleration of up to 770 kW was

#hotchi.hideaki@jaea.go.jp

ISBN 978-3-95450-178-6

achieved with no significant beam loss, but then the 1-MW beam acceleration was not reached due to an over-current of the RF anode power supply. Higher intensity beam needs larger beam loading compensation. Thus, the workload of the RF power supply increases with the ramp-up of the beam intensity.

After this beam test, a quick measure against the RF trip was taken; the resonant frequency of the RF cavity was shifted from 1.7 MHz to 2.1 MHz to decrease the anode current required for the 1-MW beam acceleration. By this treatment, the 1-MW beam acceleration was successfully achieved in January 2015. But then there still remained slight longitudinal beam loss ($<10^{-3}$) coming from a RF bucket distortion caused by beam loading. Such a beam loss occurs through a large momentum excursion, so it is mainly lost in the high dispersion area. The upper plot in Fig. 3 shows the beam loss monitor (BLM) signals in the high dispersion area at the arc section, measured over the whole acceleration time of 20 ms with various beam intensities of up to 1 MW. As shown in the figure, there is no significant beam loss up to 825 kW, but it appears when the beam intensity reaches over 900 kW. RCS employs a multi-harmonic feed-forward (FF) system for beam loading compensation, and it works very well [4]. But, at this stage, the RF anode power supply nearly reached the limit again, and there remained no enough margin for sufficient beam loading compensation for the 1-MW beam. The resonant frequency shift also contributed to this beam loss. RCS normally accelerates two bunches with the harmonic number of h=2. Thus, major parts of wake voltage components are to be the even harmonics (h=2, 4, 6). But, after the resonant frequency shift, the effect of the odd harmonics (h=1, 3, 5) was additionally enhanced, which caused a coupled-bunch-like behaviour, i.e. different longitudinal motions for two bunches [5]. Our FF system covers the odd harmonics as well as the even ones [6], but this phenomenon made the FF tuning more complicated.

After receiving this result, the RF anode power supply upgrade was carried out using the scheduled summer maintenance period in 2015. Then, the resonant frequency was also put back to the original value to make the longitudinal motion more stable. As shown in the lower plot in Fig. 3, the longitudinal beam loss was completely removed by beam loading compensation conducted in October 2015 right after the RF power supply upgrade.

Transverse Beam Loss and its Localization

Most of remaining transverse beam loss was well localized at the collimator section in the dispersion-free long straight insertion. Figure 4 shows the BLM signals at the collimator section, measured for the first 4 ms with various beam intensities of up to 1 MW. As shown in the figure, the beam loss occurs only for the first 1 ms of beam injection, and its beam loss amount simply shows a linear beam intensity dependence. They indicate that the observed beam loss mainly arises from foil scattering during charge-exchange injection. The other beam loss, such as space-charge induced beam loss, was well minimized by the combination of 100π-mm-mrad correlated transverse injection painting and longitudinal injection painting [7-9]. The beam loss for the 1-MW beam was evaluated to be <0.1%. This beam loss rate corresponds to <130 W in power, which is much less than the collimator capability of 4 kW.

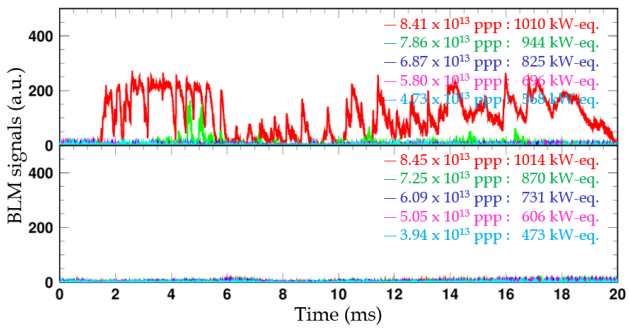

Figure 3: BLM signals in the high dispersion area measured over the whole 20 ms with various beam intensities of up to 1 MW before (upper) and after (lower) the RF power supply upgrade.

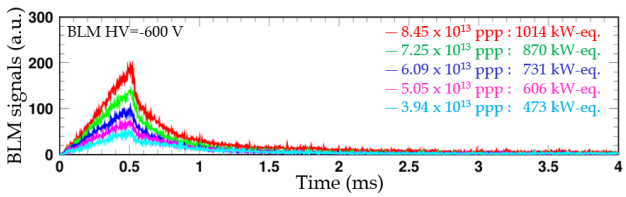

Figure 4: BLM signals at the collimator measured for the first 4 ms with various beam intensities of up to 1 MW, where 100π-mm-mrad correlated transverse injection painting and longitudinal injection painting were applied.

Beam Instability and its Suppression

Beam instability is also an important issue for the 1-MW beam acceleration. In RCS, the extraction pulse kicker is the most dominant impedance source, causing horizontal beam instability depending on the choice of the operational parameters such as the betatron tune and the chromaticity [10, 11]. Thus, for its suppression, the systematic beam instability measurement was done with different tunes and chromaticities at the initial stage of the 1-MW beam test.

Figure 5 shows six sets of tune variations from injection to extraction used for this measurement; the tunes at injection were set at the same point, but after that, they were moved differently toward extraction. Figure 6 shows the time dependence of the turn-by-turn horizontal beam position, measured for the 1-MW beam with the sets of tune variations. The green plots in this figure show the case that the natural chromaticity is fully corrected to zero at injection with dc sextupole fields. In this case, the beam instability occurs for any choice of the tune variation, whereas the growth rate displays a characteristic tune dependence, which is mainly determined by the frequency dependence of the kicker impedance. On the other hand, the red and blue plots are

ISBN 978-3-95450-178-6

the cases of less chromaticity correction; only a quarter of the natural chromaticity is corrected at injection for the blue ones, while no chromaticity correction is applied for the red ones. In this figure, one can find the beam instability is more stabilized by Landau damping through momentum spread as the negative chromaticity becomes larger. This situation allows us to fully suppress the beam instability in combination with tune control even for the 1-MW beam.

Thus, the operational condition to damp the beam instability was revealed through this measurement. Figures 3 and 4, presented above, are the experimental data taken with the stable condition, namely, with the combination of a quarter of the full chromaticity correction and Tune (4), where no instability occurs.

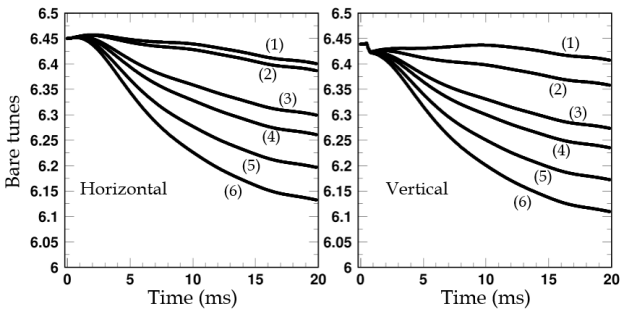

Figure 5: Six sets of tune variations from injection to extraction used for the beam instability measurement.

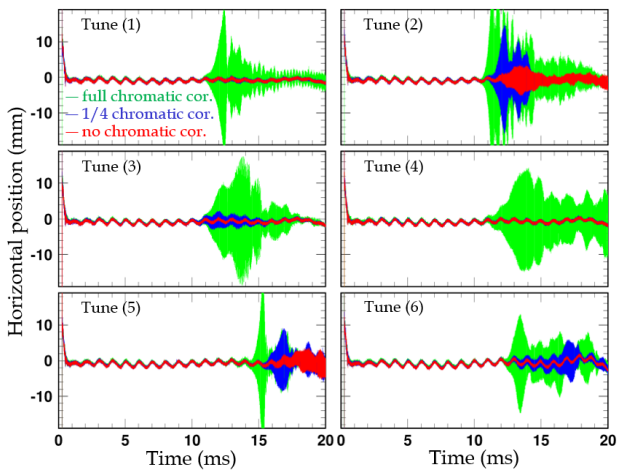

Figure 6: Time dependence of the turn-by-turn horizontal beam position measured for the 1-MW beam with six sets of tune variations (1)–(6) given in Fig. 5; (green) the natural chromaticity is fully corrected to zero at injection with dc sextupole fields, (blue) only a quarter of the natural chromaticity is corrected similarly, and (red) no chromaticity correction is applied.

FURTHER BEAM LOSS MITIGATION BY LARGER TRANSVERSE PAINTING

As already described in the last section, beam loss other than foil scattering beam loss was well minimized. Thus, the next subject is to further reduce the foil scattering beam loss. Most of the foil scattering beam loss is well localized at the collimators, so no serious problem has been encountered to date. But some of them with large scattering angles cause un-localized beam loss, making relatively high machine activation near the charge-exchange foil. It was 15 mSv/h on the chamber surface right after the 400-kW routine beam operation. This value should be 38 mSv/h if the output beam power is increased to 1 MW as is. To preserve a better hands-on-maintenance environment, the machine activation has to be reduced as low as possible.

The amount of the foil scattering beam loss is in proportion to the foil hitting rate during injection. One possible solution to reduce the foil hitting rate is to expand the transverse painting area. As described in [7], in RCS, horizontal painting is performed by a horizontal closed orbit variation during injection. Thus the foil hitting rate decreases as the horizontal painting area becomes wider, because the circulating beam more rapidly escapes from the foil thanks to the larger horizontal closed orbit variation. On the other hand, vertical painting is performed by a vertical injection angle change during injection. Vertical painting also acts to reduce the foil hitting rate through the wider painting area than the vertical dimension of the foil. The painting emittance used thus far is 100π mm mrad, where the average number of foil hits per particle is 41. This number can be reduced to 25 or 15 if the painting emittance is enlarged to 150 or 200π mm mrad.

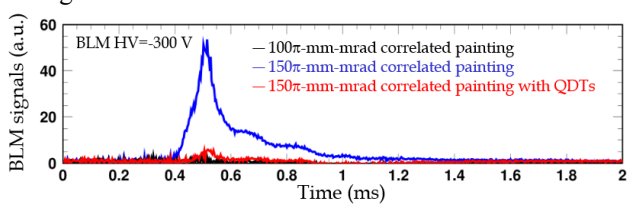

Figure 7: BLM signals at the collimator measured for the first 2 ms with a beam intensity of 850 kW.

Realizing 150π-mm-mrad Transverse Painting

Such a wide-ranging transverse injection painting had not been realized until recently due to edge focusing of pulsed injection bump magnets. The edge focus cause a 30% big beta function beating during injection. This beta function beating makes a distortion of the lattice super-periodicity and additionally excites various random betatron resonances. Such random resonances cause a shrinkage of the dynamic aperture during the injection period, leading to extra beam loss when the transverse painting area is enlarged.

To compensate the beta function beating, we recently installed six sets of pulse type quadrupole correctors (QDT1–6 in Fig. 1) [12], by which the effect of the random resonances can be minimized through the recovery of the super-periodic condition.

To confirm the effectiveness of the correction scheme, we performed a beam test with an 850-kW intensity beam [13]. As shown in Fig. 7, 0.5% significant extra beam loss

ISBN 978-3-95450-178-6

occurred when the transverse painting area was enlarged from 100 to 150π mm mrad, but the beam loss was minimized as expected by introducing QDTs.

The empirical result was well reproduced by the numerical simulation. The more detailed mechanism for the observed phenomena was investigated with the simulated result [13]. Figure 8 shows the transverse phase space coordinates calculated at the end of injection with the painting emittance of 150π mm mrad, where three kinds of transverse beam distributions are plotted; (a) without edge focus, (b) with edge focus, and (c) with the addition of QDTs to (b). In this figure, one can find that beam halo formation is enhanced from (a) to (b) by the edge focus, especially on the vertical plane. This beam halo formation causes the extra beam loss observed in the blue plot in Fig. 7. But, the beam halo is well mitigated from (b) to (c) by QDTs, which causes the beam loss reduction observed in the red plot in Fig. 7.

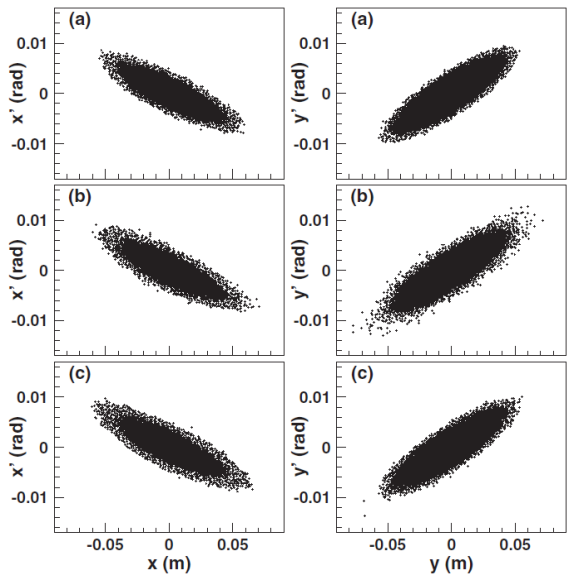

Figure 8: Two-dimensional plot of transverse phase space coordinates calculated at the end of injection with 150π-mm-mrad correlated painting, where three kinds of transverse beam distributions are plotted; (a) without edge focus, (b) with edge focus, and (c) with the addition of QDTs to (b).

Figure 9 shows a tune diagram near the present operating point. The numerical simulation confirmed the beam halo is formed through the combined effect of two resonances; $\nu_x+2\nu_y=19$ and $2\nu_x-2\nu_y=0$. The $\nu_x+2\nu_y=19$ resonance is a third-order random resonance arising from the chromatic correction sextupole field and the intrinsic sextupole field component in the main bending magnets, and it is additionally excited through a distortion of the super-periodicity caused by the edge focus during injection. This sum resonance induces emittance growth on both horizontal and vertical planes with the invariant value of $2J_x-J_y$. On the other hand, the $2\nu_x-2\nu_y=0$ resonance is a fourth-order systematic resonance, which is mainly excited through the octupole component in the space charge field. This difference resonance induces emittance exchange between the horizontal and the vertical planes with the invariant value of J_x+J_y.

Figure 10 shows a typical sample of the turn-by-turn betatron actions of one macro-particle that forms beam halo. In this figure, one can see a characteristic emittance blow-up that implies the combined effect of the two resonances; the horizontal and the vertical actions of the macro-particle gradually grow up along the line of $2J_x-J_y$ =const, while oscillating in a direction parallel to the line of J_x+J_y=const. This analysis confirmed that most of the beam halo is generated through such a single-particle behaviour. In particular, the contribution of the $\nu_x+2\nu_y=19$ resonance is more critical, since the resonance causes more severe beam halo formation on the vertical plane. QDTs act to mitigate the $\nu_x+2\nu_y=19$ resonance through the recovery of the super-periodic condition. That is, it follows that the beam loss reduction achieved in this beam test is mainly led through the mitigation of the vertical beam halo by QDTs.

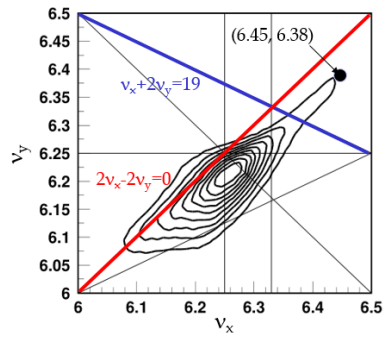

Figure 9: Tune diagram near the present operating point (6.45, 6.38), where the tune footprint was calculated at the end of injection with 150π-mm-mrad correlated painting assuming a beam intensity of 850 kW.

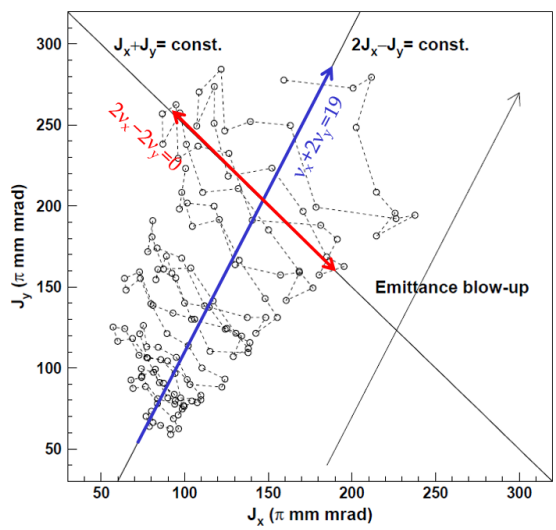

Figure 10: Typical sample of the single-particle behaviour of one macro-particle that forms beam halo; two-dimensional plot of the turn-by-turn betatron actions.

ISBN 978-3-95450-178-6

Realizing 200π-mm-mrad Transverse Painting

The above analysis gave another important suggestion. That is, the further expansion of transverse painting area can be realized by reducing the effect of the $2\nu_x-2\nu_y=0$ resonance, as well as mitigating the $\nu_x+2\nu_y=19$ resonance with QDTs. For this clue, we discussed the introduction of anti-correlated painting, instead of correlated painting used thus far.

In RCS, both correlated and anti-correlated painting are available, in which anti-correlated painting has several advantages for mitigating the effect of the $2\nu_x-2\nu_y=0$ resonance. As shown in the left plot in Fig. 11, in correlated painting, the injection beam is painted along the blue arrow. To the direction of beam painting, the emittance exchange by the $2\nu_x-2\nu_y=0$ resonance occurs in the orthogonal direction like the red arrow. Thus the emittance exchange is directly connected to the emittance growth in this case. On the other hand, in anti-correlated painting, the direction of beam painting is the same as the direction of the emittance exchange as shown in the right plot in Fig. 11. Therefore, the emittance growth caused by the emittance exchange is well suppressed in this case. Another advantage of anti-correlated painting is to make a KV-like distribution. Therefore anti-correlated painting gives less space-charge octupole field component, acting to mitigate the $2\nu_x-2\nu_y=0$ resonance.

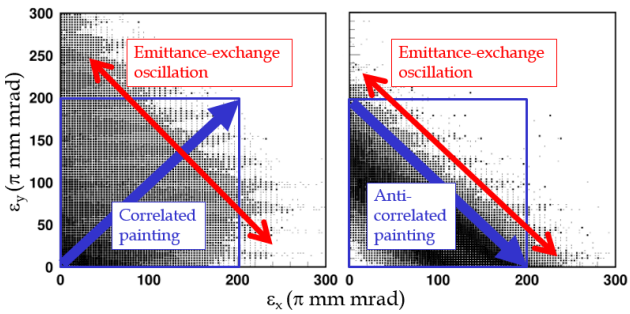

Figure 11: Two-dimensional plot of the beam emittances calculated at the end of injection with 200π-mm-mrad correlated and anti-correlated painting assuming a beam intensity of 1 MW.

Based on the above considerations, we tried to further expand the transverse painting area to 200π mm mrad for the 1-MW beam. Figure 12 shows the experimental result. The first plot (a) is the case of 200π-mm-mrad correlated painting, where 1.9% significant extra beam loss occurred. The beam loss was reduced to (b) as expected by introducing anti-correlated painting. The beam loss was further reduced to (c) by turning off the chromaticity correction, that is, by turning off the sextupole magnets. Less sextupole field mitigates the effect of the $\nu_x+2\nu_y=19$ resonance, which is the main cause of this beam loss reduction. The beam loss was finally reduced to (d) by introducing QDTs, which is caused by the further mitigation of the $\nu_x+2\nu_y=19$ resonance through the recovery of the lattice super-periodicity.

As shown in the plot (d), slight extra beam loss still remains. But we expect the remaining beam loss does not lead to serious issue, because the value is small enough; besides most of the beam loss can be localized at the collimator section. On the other hand, uncontrolled beam loss arising from large-angle foil scattering was reduced drastically by the above efforts. While the original number of foil hits per particle was 41 with 100π-mm-mrad transverse painting, it was reduced to 15 by expanding the transverse painting area to 200π mm mrad, and then to 7 by further optimizing the foil size and its position. This reduced number of foil hits expects that the machine activation near the charge-exchange foil is kept at less than 10 mSv/h on the chamber surface even for the 1-MW beam operation, which is sufficiently within the acceptable level.

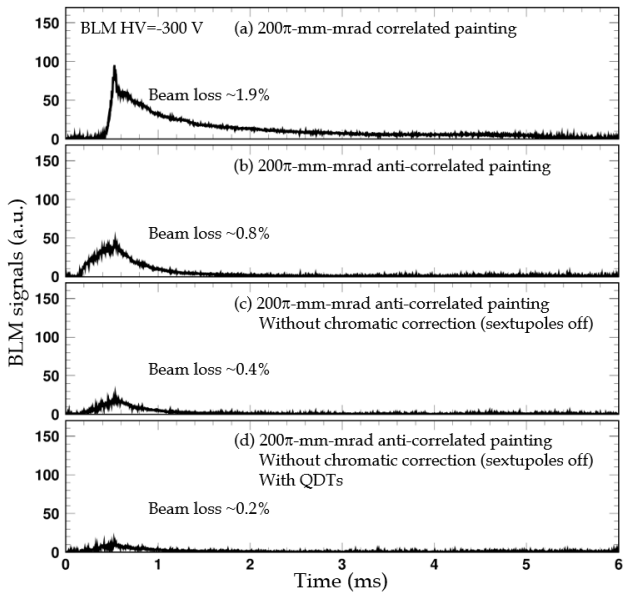

Figure 12: BLM signals at the collimator measured for the first 6 ms with a beam intensity of 1 MW.

SUMMARY

We restarted a 1-MW beam test in October 2015 after the RF power supply upgrade.

By the recent efforts, the 1-MW beam operation is now estimated to be established within a permissible beam loss level. Though it is unfortunate that the routine output beam power from RCS is now limited to 200 kW due to a malfunction of the neutron production target at MLF, RCS beam commissioning in itself is making steady progress toward realizing the routine 1-MW design beam operation.

The further parameter optimization for the 1-MW beam will be continued with more careful attention to beam quality as well as to beam loss.

REFERENCES

[1] H. Hotchi *et al.*, *Phys. Rev. ST Accel. Beams* **12**, 040402 (2009).

ISBN 978-3-95450-178-6

[2] H. Hotchi *et al.*, Prog. Theor. Exp. Phys. **2012**, 02B003 (2012).
[3] H. Hotchi, in *Proc. of HB2014*, East Lansing, MI, USA, 2014, pp. 6–11.
[4] F. Tamura *et al.*, *Phys. Rev. ST Accel. Beams* **14**, 051004 (2011).
[5] M. Yamamoto *et al.*, in Proc. of the 12th Annual Meeting of Particle Accelerator Society of Japan, Tsuruga, Japan, 2015, pp.1008–1012.
[6] F. Tamura *et al.*, *Phys. Rev. ST Accel. Beams* **18**, 091004 (2015).
[7] H. Hotchi *et al.*, *Phys. Rev. ST Accel. Beams* **15**, 040402 (2012).
[8] F. Tamura *et al.*, *Phys. Rev. ST Accel. Beams* **12**, 041001 (2009).
[9] M. Yamamoto *et al.*, *Nucl. Instrum. Methods Phys. Res.*, Sect. A **621**, 15 (2010).
[10] Y. Shobuda *et al.*, in *Proc. of HB2014*, East Lansing, MI, USA, 2014, pp. 369–372.
[11] P.K. Saha *et al.*, in *Proc. of IPAC2016*, Busan, Korea, 2016, pp. 589–591.
[12] H. Hotchi *et al.*, *Nucl. Instrum. Methods Phys. Res.*, Sect. A **778**, 102 (2015).
[13] H. Hotchi *et al.*, *Phys. Rev. Accel. Beams* **19**, 010401 (2016).

ISBN 978-3-95450-178-6